JOURNAL OF THERMOPHYSICS AND HEAT TRANSFER
Vol. 22, No. 3, July–September 2008

Unsteady Numerical Investigation of Blade Tip Leakage, Part 2: Time-Dependent Parametric Study

Patricia Phutthavong* and Ibrahim Hassan†
Concordia University, Montreal, Quebec H3G 1M8, Canada
and
Terry Lucas‡
Pratt and Whitney Canada, Longueuil, Quebec J4G 1A1, Canada

DOI: 10.2514/1.29314

The purpose of the present work is to conduct an unsteady study of the tip leakage flow adjacent to the shroud in real gas turbine engines using an in-house industrial computational fluid dynamics code. Both time-averaged and time-dependent data for the velocity, temperature, and mass flow rate in the tip clearance region are presented in parts 1 and 2, respectively. In part 2 of the present work, the effect of tip clearance height, inlet turbulence intensity, inlet total temperature, and rotor angular velocity on the tip leakage flow pattern is investigated. It is found that the separation bubble is always present near the pressure side of the blade tip at all times and that its size varies with flow conditions. For smaller tip clearance heights, the mass flow rate entering the tip clearance region is lower, due to the smaller area, which results in a smaller separation bubble. At higher stagnation temperatures, the separation bubble size is also reduced, due to the flow's higher velocity, which allows the leakage flow to dominate over the bubble growth. Also, at lower angular velocities, the effect of the shroud relative motion is reduced, and so more leakage flow is allowed to enter, thereby suppressing the growth of the separation bubble.

Nomenclature

C_x	=	blade axial chord, m
h	=	tip clearance height, m
I	=	turbulence intensity, u'/U_∞
M	=	Mach number, V/c
p	=	pressure, Pa
r	=	radial coordinate, m
T	=	temperature, K
t	=	time, s
t^*	=	nondimensional time, $t^* = t/\Theta$
U	=	velocity, m/s
u_i'	=	fluctuation of velocity from the ensemble-averaged value, m/s
$\boldsymbol{v}$	=	velocity vector $\langle u, v, w \rangle$, m/s
W	=	mass flow rate, kg/s
y	=	Cartesian coordinate oriented along the circumferential direction, m
z	=	Cartesian coordinate oriented along the radial direction, m
Δt	=	time step, s
Θ	=	airfoil passing period, s
θ	=	angular pitch, rad
Ω	=	rotor angular velocity, rpm

Subscripts

c	=	core flow
o	=	stagnation properties
rel	=	relative
∞	=	freestream conditions

Received 16 December 2006; revision received 29 October 2007; accepted for publication 6 November 2007.

*M.A.Sc. Student, Department of Mechanical and Industrial Engineering.
†Associate Professor, Department of Mechanical and Industrial Engineering, 1455 de Maisonneuve Boulevard West, Mailbox EV004.213; hassan@encs.concordia.ca (Corresponding Author).
‡Chief, Turbine Cooling and Static Structures, 1000 Marie-Victorin, Mailbox 01SA4.

I. Introduction

THE turbine stage, including the nozzle guide vane (NGV) and the rotor, will be modeled and simulated using a 3-D Reynolds-averaged Navier–Stokes finite volume code that is currently available in the aerospace industry. Description of the code, which is called Nistar, may be found in part 1 and in [1–3]. As observed from the rotating reference frame, the flow behavior inside the tip clearance region is time-dependent, due to the periodic passing of the vanes. In part 2 of this study, time-dependent simulations will be performed to investigate the effect of the tip clearance height, the inlet turbulence intensity, the inlet stagnation temperature, and the rotor angular velocity on the unsteady tip clearance flow behavior. The work of [4], described in part 1, will serve as the baseline case with which the results will be compared.

Results from the time-averaged simulation of the baseline case, presented in part 1, showed leakage flow entering the tip clearance region at the pressure side of the blade, causing the development of a separation bubble at this location. The separation bubble develops due to the sudden change in curvature as the leakage flow moves upward to negotiate the airfoil as it enters the tip clearance region. Near the pressure side of the tip clearance region and near the blade tip on the suction side, the leakage flow is dominant, whereas opposing flows entering through the suction side dominate near the shroud and at the suction side. This opposing flow is the combined effect of the shroud relative motion and the crossflow originating for the adjacent blade passage on the suction side. As a result, the circumferential and radial velocity profiles show regions of zero velocity in the tip clearance region.

The static pressure and adiabatic-wall temperature on the shroud were also obtained from the time-averaged solution. Another small recirculation region was observed above the rotor passage and was attributed to the blade passage crossflow interacting with the high-pressure region found at the suction side of the blade. This high-pressure region is caused by the combined effect of the crossflow with the shroud boundary layer flow interacting with the tip leakage flow inside the tip clearance region. In addition, the adiabatic-wall temperature decreases from the leading edge to the trailing edge in the tip clearance region, indicating the effect of the turbine expansion

process and the extraction of kinetic energy from the fluid. High adiabatic-wall temperatures were found at the leading edge of the blade tip, which indicates that high heat transfer rates will occur in this region. These high temperatures were attributed to the flow deceleration that occurs as the flow from the vane strikes the blade tip's leading edge.

In part 2, the unsteady simulation of [4] will be performed using the time-averaged solution from part 1 as an initial solution. This simulation served as a baseline case for the unsteady parametric investigation, which studied the effect of the tip clearance height, inlet turbulence intensity, inlet total temperature, and rotor angular velocity on the tip leakage flow pattern. For each case, an appropriate time-averaged solution was also obtained and was used as an initial solution for the unsteady simulation. In addition, it is important to note that it was ensured that the time-accurate solution displayed appropriate time-periodicity behavior before data were recorded. This ensured that the results will repeat themselves with each subsequent vane passing. All results presented here were recorded in the rotor's relative reference frame.

II. Problem Description

Time-accurate simulations require a huge number of computer resources. For the unsteady cases, one vane passage and two blade passages were modeled so that both the NGV and rotor domains are of equal pitch. This allows information to be transmitted appropriately through the interface during the unsteady simulation using the sliding-mesh calculations. In this case, Nistar makes an exact copy of the blade mesh used in the steady-state simulations, which significantly increases the size of the entire computational domain. The time step was chosen such that 200 time steps are required for one vane-passing period. In addition, 10 inner iterations were used for each time-step calculation. For the Nistar code, 10 inner iterations are sufficient for the numerical residuals to decrease by two orders of magnitude.

Sliding meshes are required to obtain time-accurate results for rotor-stator interaction, and is the most computationally demanding when simulating flows with multiple moving reference frames. Here, the stator flow domain and rotor flow domain are generated separately, with an interface boundary condition defined as the plane on which the stator and rotor flow domains coincide. The two interface boundaries are then used to form a grid interface, which allows the domains to move (or slide) relative to each other at this boundary. It is important to note that node alignment at the grid interface is not required.

To compute the flow data at the interface, the intersection between the interfaces is determined. If there are fluid zones on both sides of the interface, then an interior zone is created. If not, periodic zones are created. A two-dimensional example is shown in Fig. 1. Interface boundary 1 consists of faces AB and BC and belongs to flow domain 1. Similarly, interface boundary 2 resides in flow domain 2 and contains faces DE and EF. The intersection of both flow domains yields faces ad, db, be, ec, and cf. If there is flow on both sides of the intersection (that is, where the two flow domains overlap), db, be, and ec are grouped to form an interior zone and the remaining faces ad and cf form periodic zones. Thus, the flux across the grid interface from cells I and II to cell IV is computed using faces db and be.

Because data are recorded in the rotating reference frame, the time periodicity of the results should be equal to the time between consecutive vane passings or the vane-passing periods. The time-accurate results were presented at four different times normalized by the vane-passing period. The nondimensional time variable t^* is defined as follows:

$$t^* = \frac{t}{\Theta_{\text{vane}}} \tag{1}$$

where Θ_{vane} is the vane-passing period obtained from

$$\Theta_{\text{vane}} = \frac{\theta_{\text{vane}}}{\Omega} \tag{2}$$

where θ_{vane} represents the vane angular pitch and Ω is the rotor angular velocity. The relative positions of the NGV and the rotor are shown in Fig. 2. Note that because the number of vane airfoils is half of the number of airfoils in the rotor, the relative positions of the NGV and rotor are identical at $t^* = 0.25$ and 0.75, as well as at $t^* = 0.50$ and 1.00.

To further demonstrate the importance of performing time-dependent simulations for blade tip leakage flow, the relative y-velocity profiles obtained at $x/C_x = 48\%$ (along the camber line and at different times in the tip clearance region) are compared with those obtained in the time-averaged solution in Fig. 3. It can be seen that the time-averaged profile provides a good approximation of the time-dependent solution, because it falls between the solutions at $t^* = 0.25$ and 0.75. However, the time-averaged solution fails to capture the high velocity obtained at $t^* = 0.25$ and 0.50 in the upper portion of the tip clearance region. The ability to capture these high velocities is important for predicting the high heat transfer rates on the shroud; thus, time-dependent solutions should be used for studying flow and heat transfer mechanisms in the tip clearance region.

It is also important to note that the shroud is stationary in the absolute reference frame. However, the results obtained in the present study are in the rotating reference frame, and because there is no postprocessor for Nistar, it was not possible to obtain

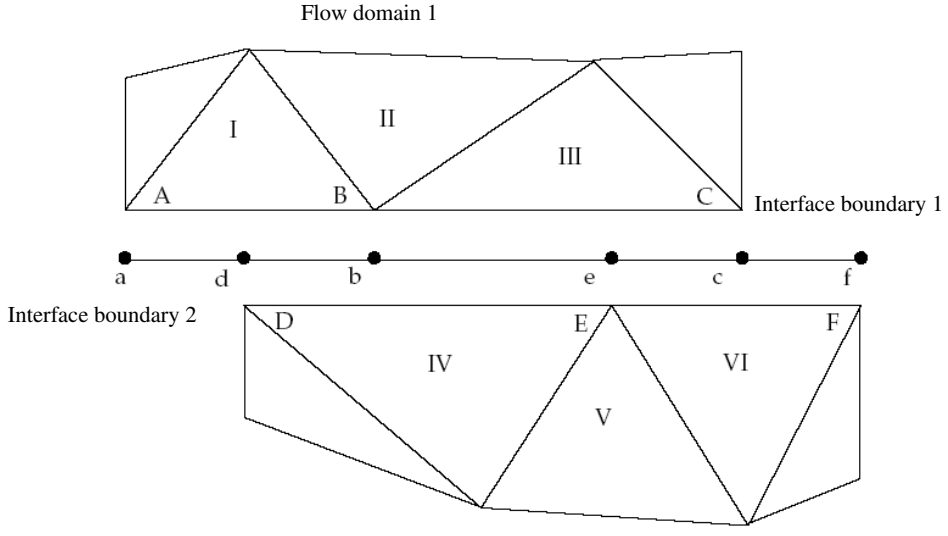

Fig. 1 Grid interface in two dimensions [2].

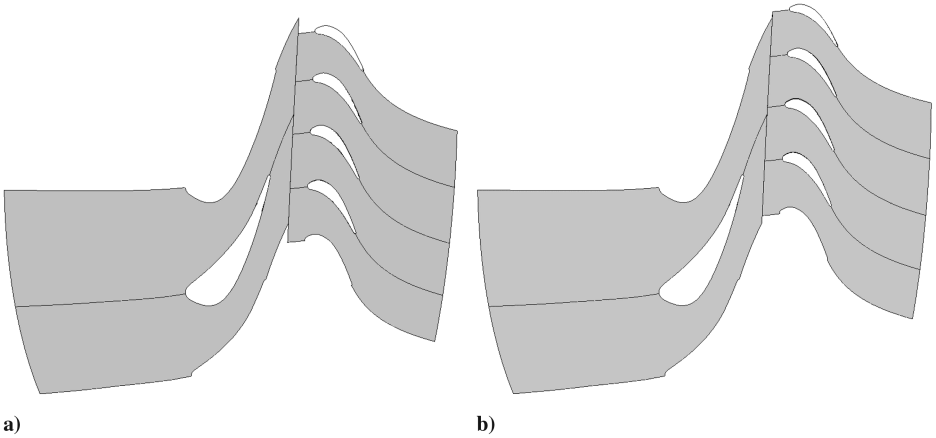

Fig. 2 Relative positions of the NGV and rotor at: a) $t^* = 0.25$ and 0.75 and b) $t^* = 0.50$ and 1.00.

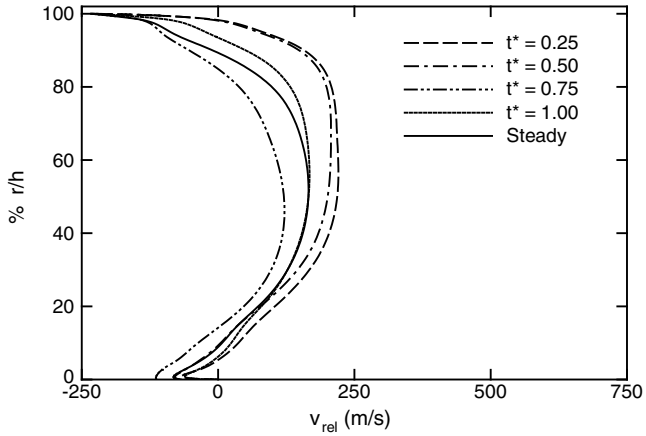

Fig. 3 Comparison of the relative y-velocity profiles at $x/C_x = 48\%$ (along the camber line and at different times) with those obtained with the time-averaged solution.

time-accurate results of the shroud as seen from the absolute reference frame. Thus, the results for the shroud (Figs. 4 and 5) were recorded at the K plane just below the shroud and are thus still in the rotor reference frame. Because the heat transfer to the shroud is determined by the flow physics and temperature just below the shroud, this information is still useful for further understanding heat transfer mechanisms to the shroud.

For the unsteady investigation, a total of eight cases were simulated, as shown in the test matrix (Table 1). The test parameters were chosen such that significant differences from the baseline results could be observed. In case 1, a tip clearance of $h = 0.6$ mm was chosen, because tip clearances are usually smaller than 1.2 mm. In addition, a tip clearance of 2.0 mm was chosen in case 2 to study the effect of larger tip clearances. The inlet turbulence intensity is defined as $I = u'/U_\infty$, and an intensity of 0.5% was chosen for case 3. This value is quite low, but previous studies [5] have also used similar values to study secondary flow in gas turbines. Higher inlet stagnation temperatures of $T_o = 600$ and 800 K were used in cases 4 and 5, because it is desirable to increase the inlet turbine temperatures to improve the efficiency of the engine. Finally, angular velocities of $\Omega = 7500$ and 11,500 rpm were chosen in cases 6 and 7 to study the effect of rotor angular velocity.

III. Results and Discussion

A. Baseline Case

Figure 4 shows the static-pressure contours just below the shroud for the baseline case. At all times, the recirculation zone at the trailing edge of the airfoil was observed. This is the result of the leakage flow, moving from the pressure side to the suction side, interacting with the

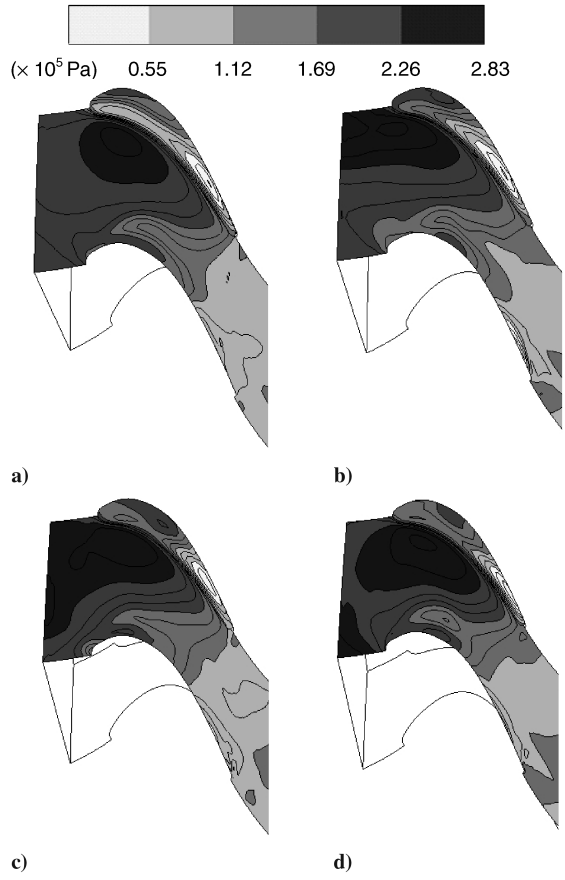

Fig. 4 Static-pressure contours below the shroud for the baseline case at different times: a) $t^* = 0.25$, b) $t^* = 0.50$, c) $t^* = 0.75$, and d) $t^* = 1.00$.

opposing rotor passage flow originating from the pressure side of the adjacent blade at the suction side of the blade tip. The recirculation is more apparent near the trailing edge, because the distance between the pressure side and the suction side of the blade tip is smallest at the trailing edge. At $t^* = 0.25$, a low-pressure region was observed in Fig. 4a in the tip clearance region at the pressure side of the blade, which shows the separation bubble development as the leakage flow enters the tip clearance region. As time progresses, a high-pressure region begins to develop and grow at the suction side near the leading edge, and this is due to the crossflow in the passage interacting with the leakage flow leaving the tip clearance region. At $t^* = 0.75$, a small recirculation zone was observed at the leading edge and at the suction side. At this time, the pressure is very high at the inlet of the shroud, because the NGV passage is now upstream of the blade, allowing most of the flow leaving the vane to enter the rotor passage.

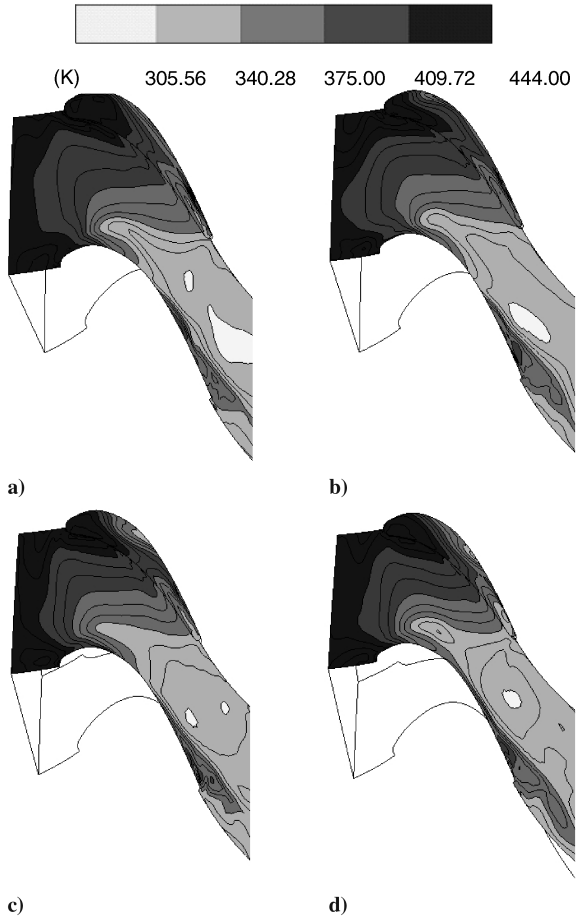

Fig. 5 Static-temperature contours below the shroud for the baseline case at different times: a) $t^* = 0.25$, b) $t^* = 0.50$, c) $t^* = 0.75$, and d) $t^* = 1.00$.

As a result, the leakage flow leaving the tip clearance region at the leading edge is obstructed by this high-pressure flow at the inlet, causing the recirculation zone to form. In the rotor passage, high-pressure regions just below the pressure side of the blade were observed at all times. However, their size and location vary, due to the passing of the vane just upstream of the rotor. From $t^* = 0.25$ to 0.50, the high-pressure region grows and extends toward the inlet of the rotor. This is due to the fact that the vane passage starting to pass by the blade. As already mentioned, at $t^* = 0.75$, the vane passage is upstream of the blade, and thus the high-pressure region is largest, because the high-pressure flow is entering the rotor from the NGV. At $t^* = 1.00$, the vane begins to pass over the rotor passage and so the accelerating flow from the vane airfoil is entering the rotor passage, thus generating low-pressure at the inlet of the rotor. This low-pressure region continues to grow, as seen from Fig. 4a, until the vane passage passes over once again.

The static-temperature contours just below the shroud for the baseline case are shown in Fig. 5. The static temperature is high at the inlet of the rotor and decreases in the axial direction as the flow

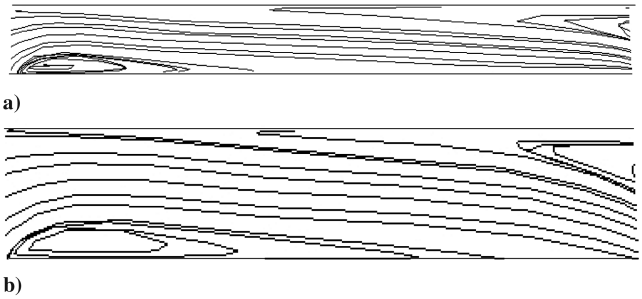

Fig. 6 Streamlines inside tip clearance region at $t^* = 0.25$ for a) case 1 and b) case 2.

accelerates through the rotor, due to energy conservation. High heat transfer rates to the shroud are the result of high adiabatic-wall temperatures. The static temperature shown here can be considered to be the adiabatic-wall temperature, because the data are recorded so close to the shroud. Thus, it can be seen that high heat transfer rates will occur in the tip clearance region near the leading edge of the blade, and this has been observed in previous studies, including Chana and Jones [6]. The region of high temperature in the tip clearance is largest at $t^* = 0.25$, because there is very little leakage flow resisting the flow near the shroud. At $t^* = 0.50$, the high-temperature region near the leading edge begins to decrease as the leakage flow begins to accelerate through the tip clearance region, attaining its smallest size at $t^* = 0.75$. At $t^* = 1.00$, the high-temperature region starts to grow again, due to the dissipation of the leakage flow.

B. Effect of Tip Clearance Height

It was observed that the separation bubble in case 2 spans nearly the entire span of the tip clearance region from the pressure side to the suction side at all times, shown in Fig. 6b. Because the tip clearance is large, the leakage flow is able to dominate a larger portion of the tip clearance region. Thus, the leakage flow moves more horizontally and is only directed downward by the opposing flow near the suction side, instead of near the pressure side as in other cases. Also, more mass flow enters the tip clearance region because the height is larger. On the other hand, the separation bubble in case 1 remains confined to the pressure side of the tip leakage region, as shown in Fig. 6a, because the mass flow rate entering the gap is much lower than the smaller gap size.

Comparison with the baseline case of the mass flux entering the pressure side of the tip clearance region at midspan is shown in Fig. 7. As expected, less mass flow enters the tip clearance region for the smaller tip clearance case, and more mass flow enters for the larger tip clearance case. From Fig. 7, it can be seen that all times, the same amount of mass flow is entering the pressure side at all locations for tip clearances. It is also interesting to note that the recirculation at the trailing edge for both tip clearances occurs at $x/C_x = 82\%$. At this location, mass flow is leaving the pressure side, as indicated by the negative flow rates from $x/C_x = 82\%$ to the trailing edge. This shows that at the midspan, the development of the recirculation zone does not depend on the tip clearance height, which makes sense because the flow conditions outside the tip clearance region have not

Table 1 Test matrix for the unsteady parametric investigation

Parameter	Case number	h, mm	I, %	T_o, K	Ω, rpm
	Baseline	1.2	3	444	9500
Effect of tip clearance height, h	1	0.6	3	444	9500
	2	2.0	3	444	9500
Effect of vane inlet turbulence intensity, I	3	1.2	0.5	444	9500
Effect of inlet stagnation temperature, T_o	4	1.2	3	600	9500
	5	1.2	3	800	9500
Effect of rotor angular velocity, Ω	6	1.2	3	444	7500
	7	1.2	3	444	11,500

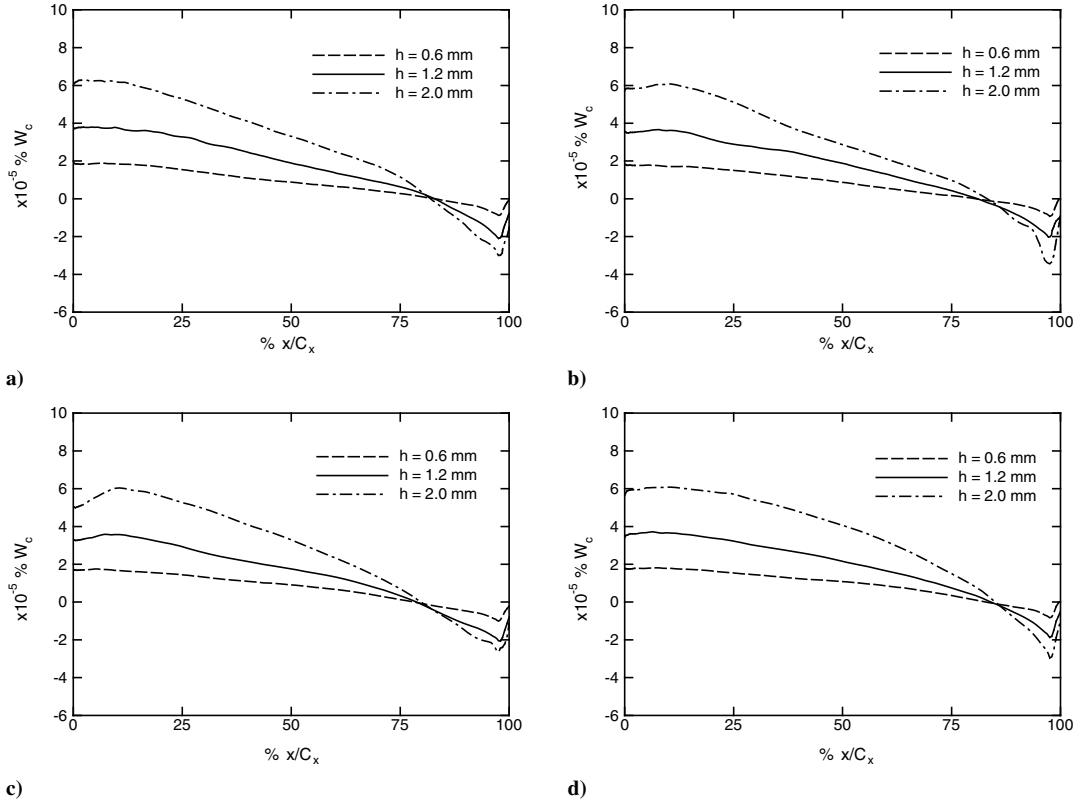

Fig. 7 Comparison of the mass flow rate entering the pressure side of the blade at different tip clearance heights at the midspan of the tip clearance region and at times: a) $t^* = 0.25$, b) $t^* = 0.50$, c) $t^* = 0.75$, and d) $t^* = 1.00$.

been modified. The secondary crossflow originating from the adjacent blade passage remains the same and interacts with the leakage flow from the smaller tip clearance region in the same manner as in the baseline case.

The mass flow rates leaving the tip clearance region through the suction side for case 1, case 2, and the baseline cases are shown in Fig. 8. Negative flow rates indicate flow leaving the suction side. At all times, there is very little flow leaving the suction side between

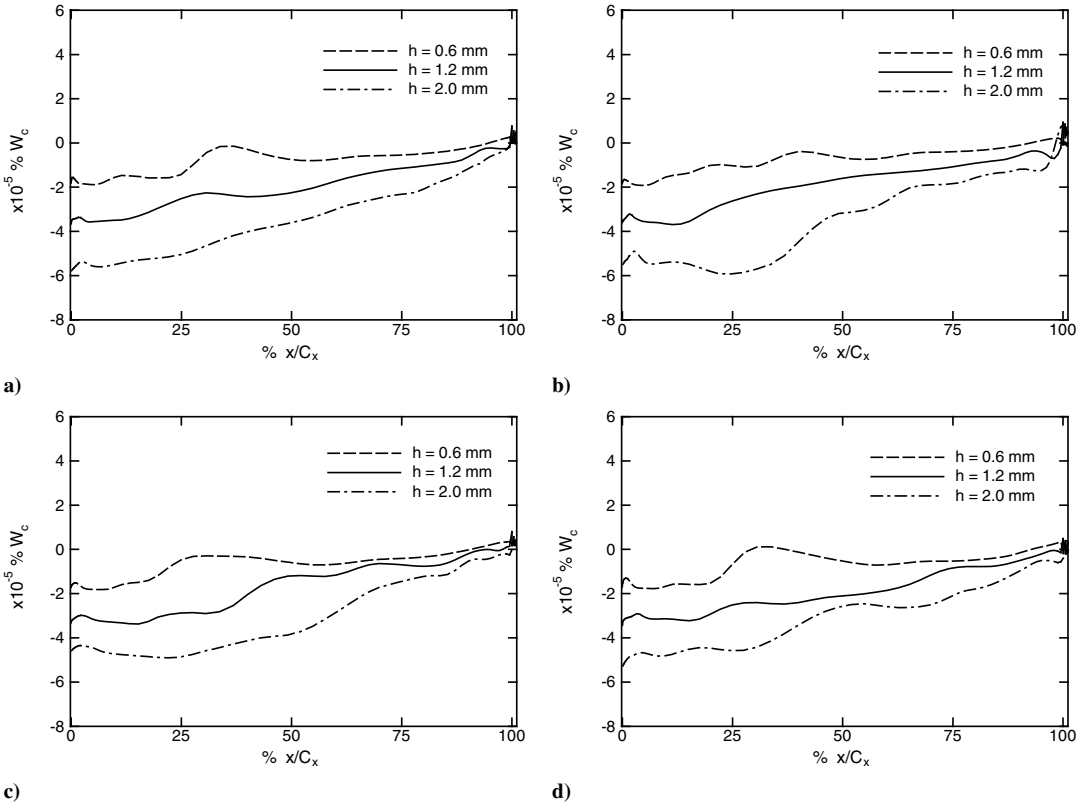

Fig. 8 Comparison of the mass flow rate entering the suction side of the blade at different tip clearance heights at the midspan of the tip clearance region and at times: a) $t^* = 0.25$, b) $t^* = 0.50$, c) $t^* = 0.75$, and d) $t^* = 1.00$.

29–36% x/C_x. In fact, at $t^* = 1.00$, the mass flow rates between 29–36% x/C_x are positive, indicating backflow into the tip clearance region. This can be explained by the fact that the thickness of the airfoil is greatest within this region. Because less mass flow enters the tip clearance region, the leakage flow has less inertia to overcome the shroud boundary-layer flow, in which the airfoil thickness is largest. The leakage flow instead deviates toward paths of least resistance, in which the airfoil thicknesses are smaller, which explains why more leakage flow leaves the suction side upstream and downstream of this region.

Figure 9 shows the relative y-velocity profiles along the camber line at different axial positions in the tip clearance region at $t^* = 1.00$. Near the leading edge, the y-velocity profiles are similar, with maximum velocities of approximately 250 m/s, because the leakage flow sees the same pressure drop before entering the tip clearance region. Near the shroud at $r/h = 66\%$, the boundary layer is less steep for the smaller tip clearance case, because the separation bubble stretches higher in the tip clearance region. Thus, the leakage flow is slower in the upper portion, because the leakage flow has to negotiate over the separation bubble for the smaller tip clearance case (case 1). At $x/C_x = 48\%$, it can be seen that the leakage flow velocity is higher for the large tip clearance case (case 2) in the upper portion of the tip gap, as mentioned before. Similarly, the velocity inside the separation bubble is larger for case 2. It is important to note that at the trailing edge, the pressure side and suction side nearly coincide with each other because the airfoil is thinnest near the trailing edge. In Fig. 9c, it can be seen that the velocity is nearly zero, because the leakage flow decelerates as it encounters the opposing flow from the suction side. Small recirculation was observed near the blade tip for the baseline case and case 1, due to the interaction of the radially downward leakage flow with the opposing flow from the suction side. On the other hand, in case 2, the velocity is positive (moving from the pressure side to the suction side) from $r/h = 4$ to 44%, which represents the high velocity inside the separation bubble, which spans from the pressure side to the suction side.

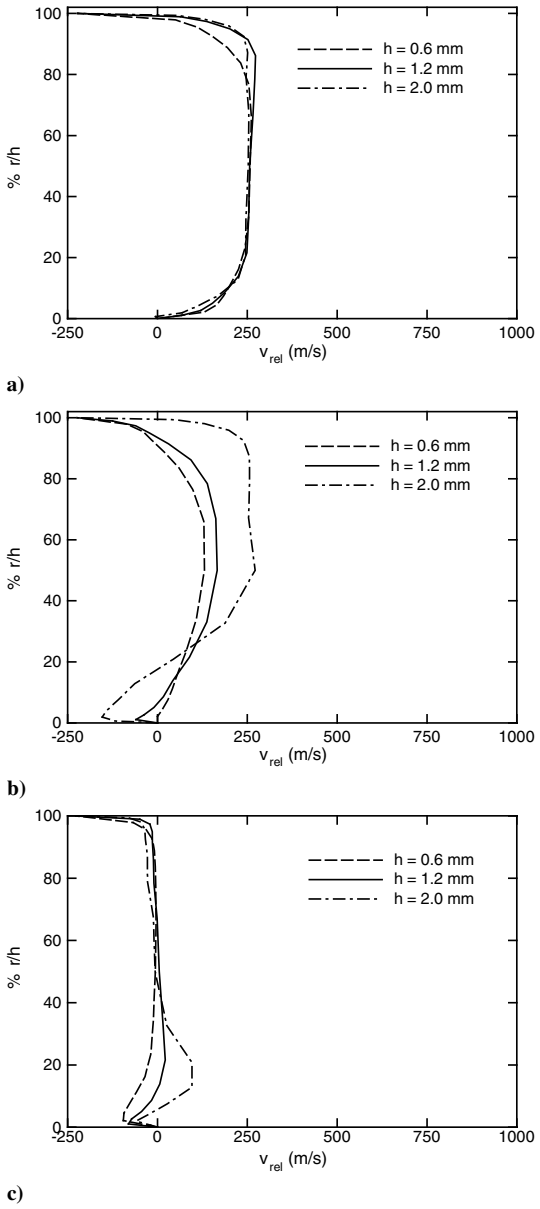

Fig. 9 Relative y-velocity profiles along the camber line for different heights at $t^* = 1.00$ at a) $x/C_x = 5\%$, b) $x/C_x = 48\%$, and c) $x/C_x = 95\%$.

C. Effect of Turbulence Intensity

It was observed that the axial component of velocity in the tip clearance region is greater in case 3 than it is in the baseline case, shown in Fig. 10. This was attributed to more flow particles accelerated through the NGV, because they have less random motion when $I = 0.5\%$. At $t^* = 0.25$, 0.75, and 1.00, it can be seen that the relative x velocity component for case 3 is indeed greater than that for the baseline case. The maximum difference occurs at $t^* = 0.75$, where the velocity at the midspan is 214 m/s for the baseline case and 256 m/s for case 3. Because the vane is in line with the blade at this time, the maximum amount of flow is allowed to enter the tip clearance region, because much of the high-pressure flow from the NGV is now located at the pressure side of the blade.

Figure 11 shows the relative Mach number distribution along the camber line in the tip clearance region at midspan at different times. From the leading edge to midchord, it can be seen that the Mach number in case 3 decreases, whereas the flow increases to sonic values for the baseline case at $t^* = 0.25$. This may be due to the flow having less random motion, and so more fluid particles from the bulk flow will make contact with the leading edge of the blade, thus decelerating the flow as it approaches the rotor. Meanwhile, at $t^* = 0.75$, it can be seen that the velocity distribution in case 3 remains relatively the same, whereas the velocity decreases for the baseline case. Because the flow has less random motion, the flowfield is less susceptible to change over time. At this time, the vane and blade are aligned with each other, and so more high-pressure flow from the NGV is entering the tip clearance region, which decreases the velocity. In addition, it was observed that the Mach number distributions for both cases follow the same trend at all times, whereby the Mach number increases to peak values at approximately $82\% x/C_x$ and then abruptly decreases at the trailing edge. This is due to the presence of the recirculation region caused by the leakage flow interaction with the crossflow from the adjacent blade passage. Thus, the peak Mach number signifies the middle of the recirculation region. Also, near the trailing edge, the velocity in case 3 increases because axial velocity increases, due to the flow having less random motion, and so the particles are able to accelerate as they leave the rotor.

D. Effect of Inlet Stagnation Temperature

At higher inlet stagnation temperatures, it was observed that the separation bubble on the pressure side is smaller than that in the baseline case. Because the stagnation temperatures are higher, the fluid's density is less and so the velocity will be significantly larger, to conserve the mass flow rate. Because the fluid has a higher velocity, the flow will reduce the size of the separation bubble. The higher-velocity flow allows the leakage flow to also overcome the opposing crossflow at the suction side; thus, there is no recirculation at the suction side.

Figure 12 shows the static-temperature distribution on the camber line at the midspan of the tip clearance region. At $t^* = 0.25$, the temperature decreases near the leading edge for cases 4 and 5, whereas it increases for the baseline case. This can be seen in the Mach number distribution on the camber line at the midspan of the tip

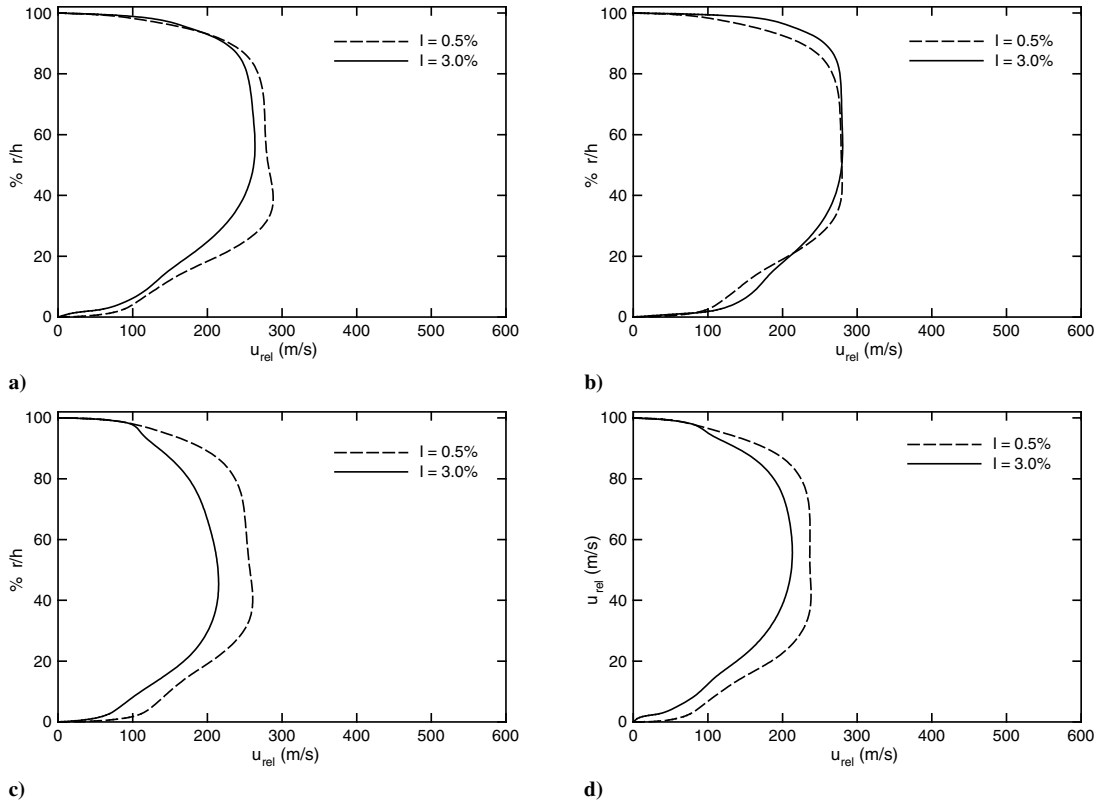

Fig. 10 Comparison of the relative x-velocity profiles at different inlet turbulence intensities at approximately $x/C_x = 48\%$, on the camber line of the blade tip and at times: a) $t^* = 0.25$, b) $t^* = 0.50$, c) $t^* = 0.75$, and d) $t^* = 1.00$.

clearance region, as shown in Fig. 13a. In addition, from Fig. 12, it was observed that the temperature decreases to a minimum value near the trailing edge at approximately $82\% x/C_x$ for both cases, and this minimum value indicates the center of the recirculation region. Thus, it was concluded that the location of the recirculation zone is independent of the inlet stagnation temperature. In Fig. 13, it can be seen that near the trailing edge, the Mach number distributions follow the same trends for all cases. In addition, the magnitudes of the Mach

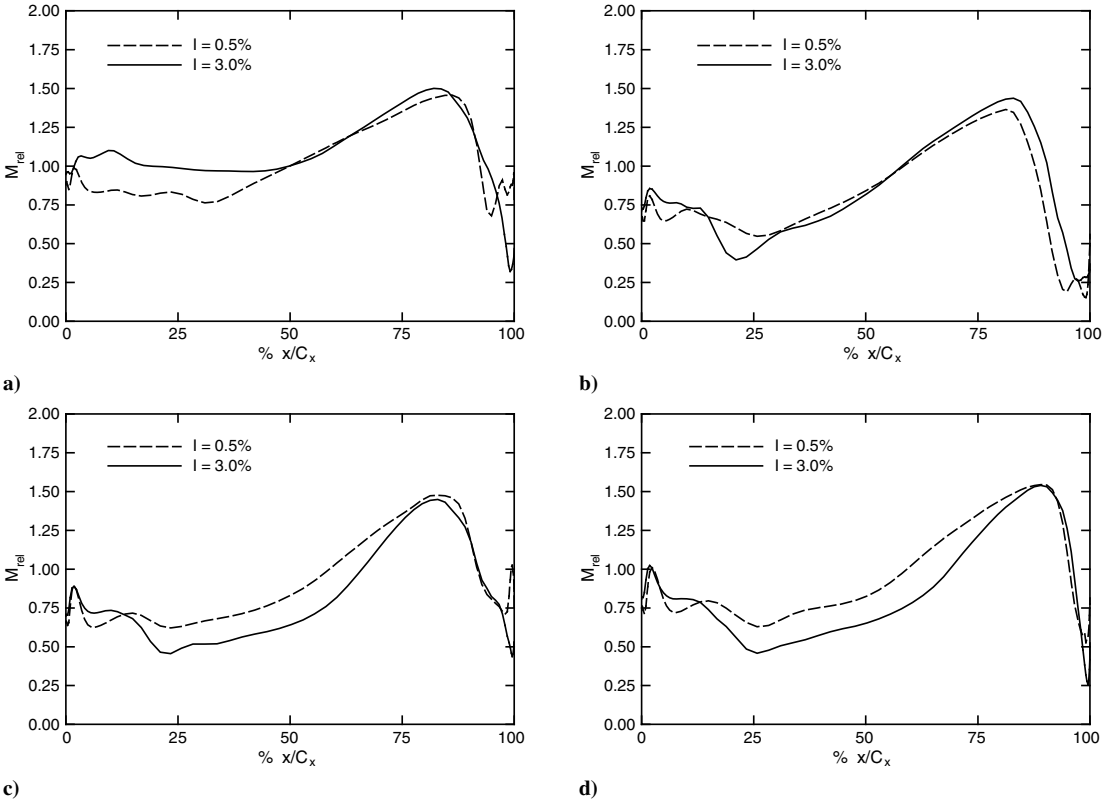

Fig. 11 Comparison of the variation of the relative Mach number with axial distance at inlet turbulence intensities at the midspan of the tip clearance region, on the camber line of the blade tip and at times: a) $t^* = 0.25$, b) $t^* = 0.50$, c) $t^* = 0.75$, and d) $t^* = 1.00$.

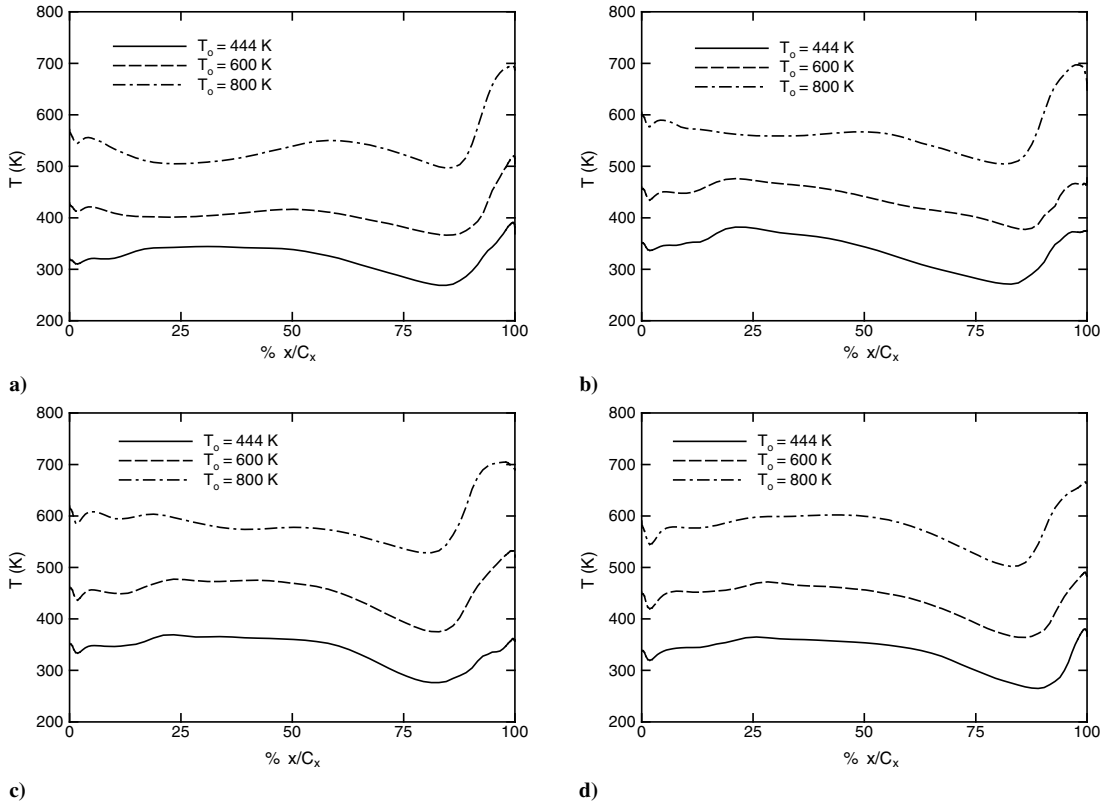

Fig. 12 Comparison of the variation of the temperature with axial distance at different inlet stagnation temperatures at the midspan of the tip clearance region, on the camber line of the blade tip and at times: a) $t^* = 0.25$, b) $t^* = 0.50$, c) $t^* = 0.75$, and d) $t^* = 1.00$.

numbers are comparable, once again indicating that the development of the recirculation zone at the trailing edge is independent of the inlet stagnation temperature. At all times, however, the Mach numbers are higher for cases 4 and 5 from the leading edge until the beginning of the recirculation zone. This is due to the fact that the flow has higher velocity in cases 4 and 5.

The relative y-velocity profiles at different axial positions and at $t^* = 1.00$ are compared in Fig. 14. Near the leading edge, the

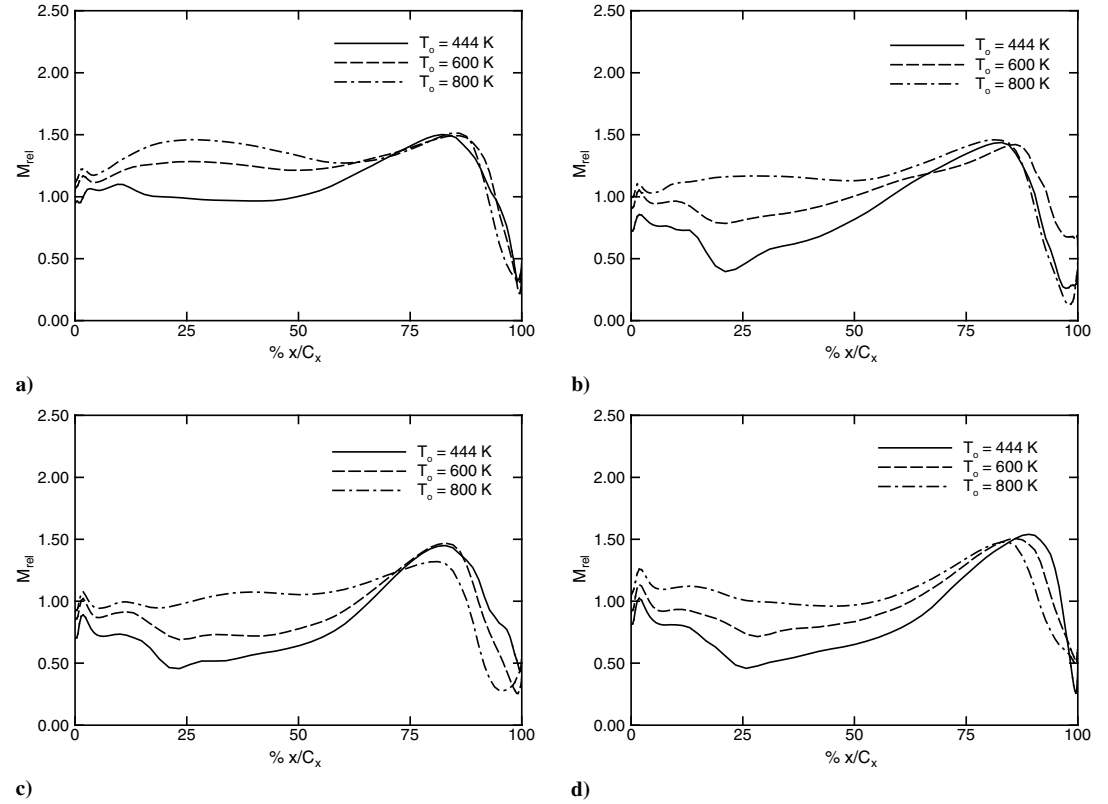

Fig. 13 Comparison of the variation of the relative Mach number with axial distance at the midspan of the tip clearance region, at different inlet stagnation temperature and at times: a) $t^* = 0.25$, b) $t^* = 0.50$, c) $t^* = 0.75$, and d) $t^* = 1.00$.

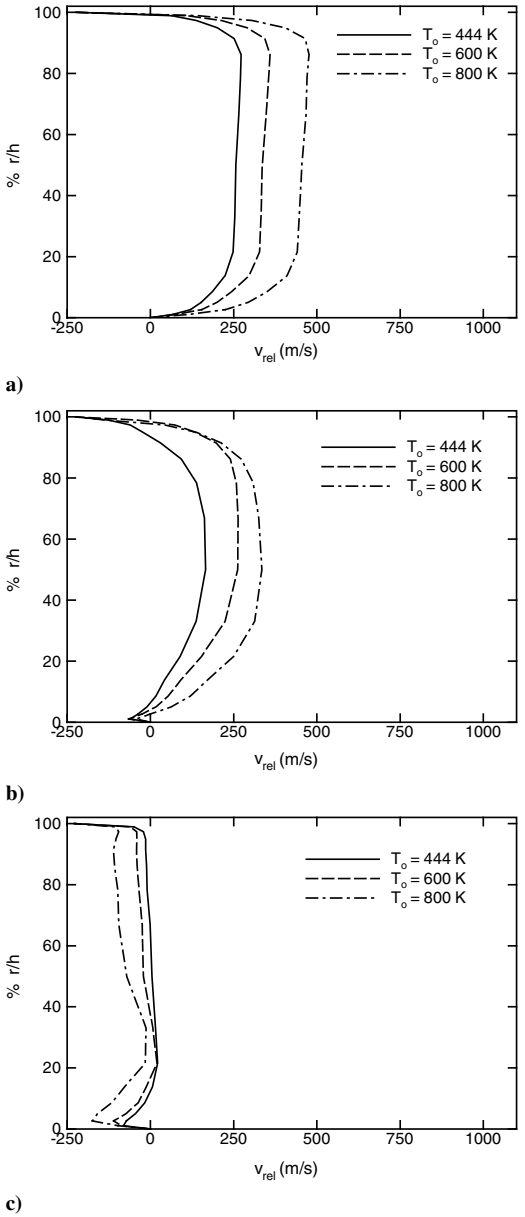

Fig. 14 Relative *y*-velocity profiles along the camber line for different stagnation temperatures at $t^* = 1.00$ at a) $x/C_x = 5\%$, b) $x/C_x = 48\%$, and c) $x/C_x = 95\%$.

velocity profiles are similar for all cases, in which higher stagnation temperatures generate higher velocities. At $x/Cx = 48\%$ in the baseline case, the opposing flow originating from the suction side is completely dominant from $r/h = 93\%$ to the shroud, which can be observed from the negative values of the y velocity in Fig. 14b. This is due to the larger separation bubble that is generated in the baseline case, because the stagnation temperature is lowest. The y velocity decreases as the leakage flow negotiates around the separation bubble. Near the trailing edge, the y velocity is nearly zero for the baseline case, because the flow is moving in the radial direction, due to the larger separation bubble. Also, near the blade tip, the opposing flow is dominant because the velocity of the opposing flow is also higher.

E. Effect of Rotor Angular Velocity

At lower angular velocities (case 6), the separation bubble is smaller when compared with the baseline case, and no recirculation at the suction side was observed. Because the rotor angular velocity is lower, this means that in the rotating reference frame, the shroud wall is moving at a lower velocity. As a result, the effect of the shroud relative motion is reduced, thereby generating less resistance to the leakage flow and a smaller separation bubble. In addition, the mass flow entering the tip clearance region will be greater, because more flow will be allowed to enter, because the separation bubble is smaller and there is less resistance from the shroud relative motion. It was also found that the recirculation region occurs at nearly the same location: at approximately $x/C_x = 82\%$.

At higher rotor angular velocities, a large separation bubble was observed, which is the result of the faster moving shroud creating more opposition for the leakage flow. Consequently, recirculation regions at the suction side near the blade tip are observed, because the leakage flow has a radially downward motion, because it must negotiate over the large separation bubble. At time progresses, it was observed that the velocity decreases above the separation bubble, due to the higher relative velocity of the shroud opposing the leakage flow. In addition, as expected, the mass flow is less for the higher rotor angular-velocity case, as can be seen from Fig. 15.

Figure 16 shows the relative y-velocity profiles at $x/C_x = 48\%$ and on the camber line in the tip clearance region for case 6 and the baseline case. At $t^* = 0.25$, 0.75, and 1.00, the leakage flow velocity in the circumferential direction is greater for case 6, as expected, because the shroud relative motion is lower than that in the baseline case. At $t^* = 0.50$, however, the leakage flow velocity near the shroud decreases, due to the high-pressure region located on the suction side near the shroud. Because the leakage flow reaches the suction side sooner, the interaction with the opposing crossflow happens at an earlier time, thus generating the high-pressure region at $t^* = 0.50$ instead of $t^* = 0.75$ for the baseline case. For the higher rotor angular-velocity case (case 7), it was observed that the y-velocity profiles are nearly identical at all times. The y velocity is lower than that of the baseline case near the shroud, due to the higher relative motion of the shroud opposing the leakage flow.

Figure 17 shows the y-velocity profiles at different axial locations at $t^* = 1.00$. Near the leading edge, the velocity is lower, due to the high velocity of the shroud, which opposes the leakage flow. At $x/C_x = 48\%$, the y velocity increases slightly for case 7 in the midspan region, because the leakage flow becomes dominant. For the lower rotor angular-velocity case, however, the y velocity is higher, because the separation bubble is much smaller. Thus, most of the leakage flow is moving toward the suction side instead of being recirculated inside the separation bubble. Near the trailing edge, the effect of the opposing flow is greater for the lower rotor angular-velocity case, because the opposing flow from the suction side is not obstructed by a large separation bubble.

IV. Conclusions

In the present study, time-averaged and time-accurate simulations were performed to numerically study the tip leakage flow behavior inside an existing gas turbine facility. More particularly, the time-accurate simulations were used in a parametric investigation to study the effect of the tip clearance height, the inlet turbulence intensity, the inlet stagnation temperature, and the rotor angular velocity on the tip leakage flow. To the best of the authors' knowledge, time-accurate (unsteady) simulations have not been performed to study the effects of flow parameters on the aerodynamics in the tip clearance region.

For the time-accurate solutions, it was found that the separation bubble is always present near the pressure side of the blade tip at all times and that its size varies with flow conditions. For smaller tip clearance heights, the mass flow rate entering the tip clearance region is lower, due to the smaller area, which results in a smaller separation bubble. At higher stagnation temperatures, the separation bubble size is also reduced, due to the flow's higher velocity, which allows the leakage flow to dominate over the bubble growth. Also, at lower angular velocities, the effect of the shroud relative motion is reduced, and so more leakage flow is allowed to enter, thereby suppressing the growth of the separation bubble.

The combined effects of the opposing crossflow from the adjacent blade passage and the shroud relative motion dominate the leakage flow from the midspan to the shroud in the tip clearance region. As

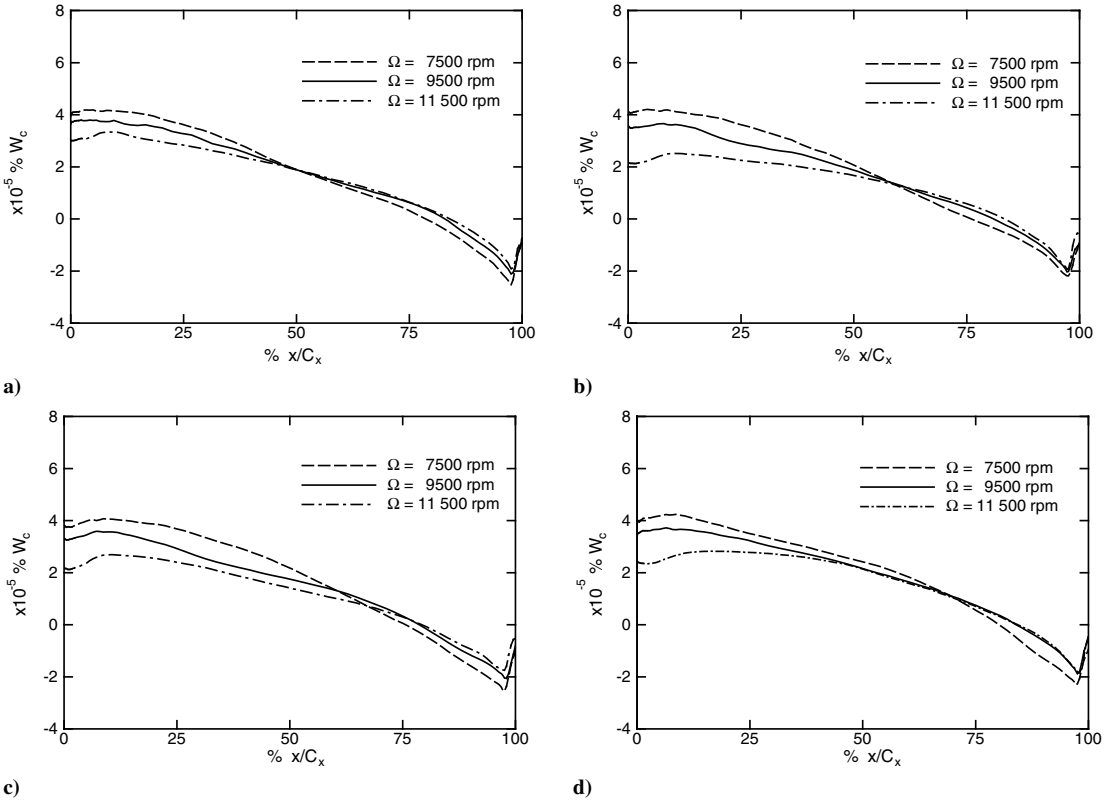

Fig. 15 Comparison of the mass flow rate entering the pressure side of the blade at different rotor angular velocities at the midspan of the tip clearance region and at times: a) $t^* = 0.25$, b) $t^* = 0.50$, c) $t^* = 0.75$, and d) $t^* = 1.00$.

time progresses, the opposing flow moves closer to the pressure side of the tip clearance region. Near the pressure side of the blade tip, the leakage flow dominates, and so the opposing flow changes direction, generating a large recirculation region from approximately $x/C_x =$ 82% to the trailing edge for all cases. It was therefore concluded that the development of this recirculation region does not depend on flow conditions, but rather on the airfoil geometry (in particular, where the airfoil thickness is smallest). The size of the recirculation region

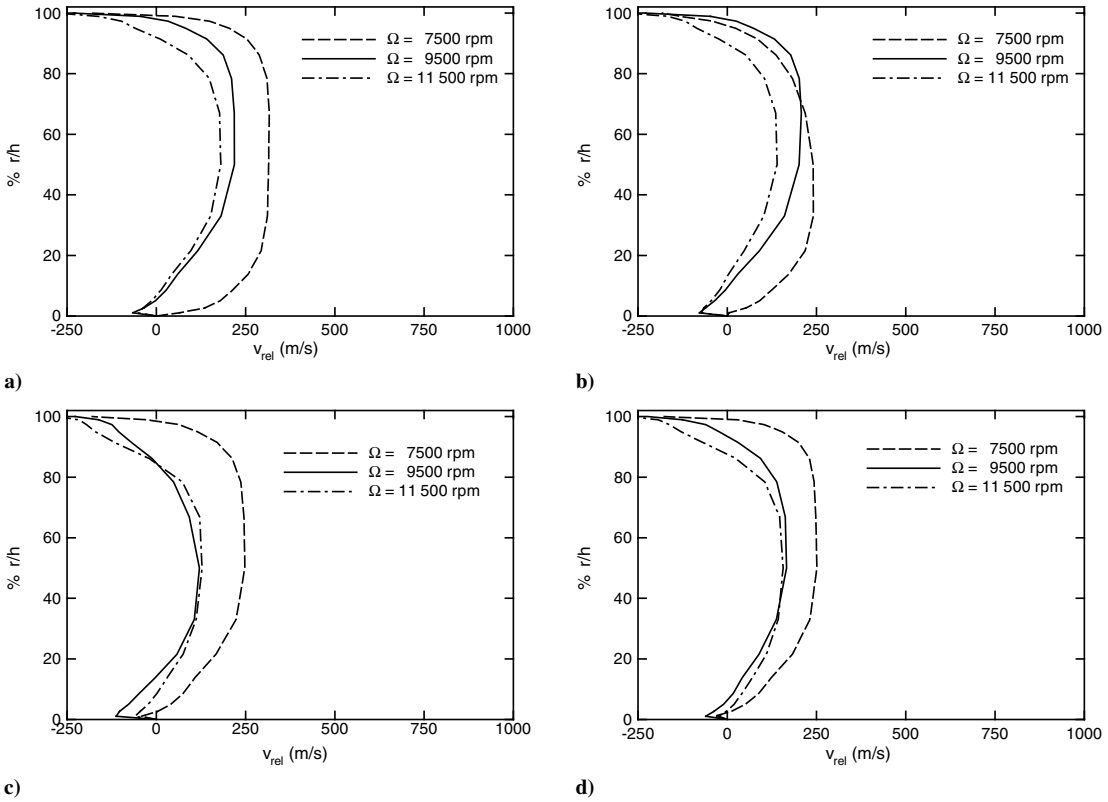

Fig. 16 Comparison of the relative y-velocity profiles at different rotor angular velocities at approximately $x/C_x = 48\%$, on the camber line of the blade tip and at times: a) $t^* = 0.25$, b) $t^* = 0.50$, c) $t^* = 0.75$, and d) $t^* = 1.00$.

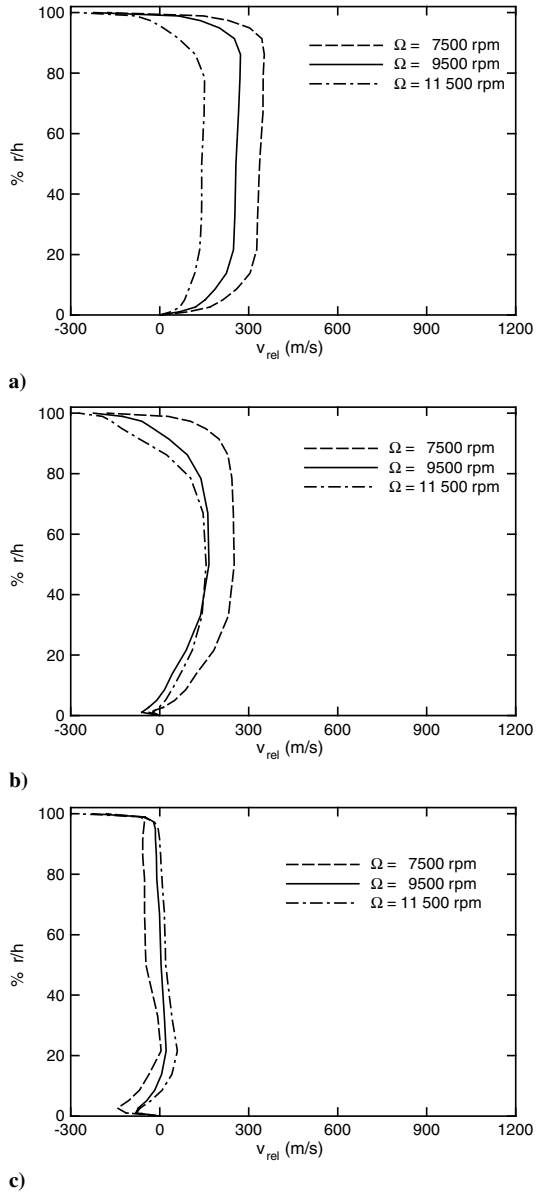

Fig. 17 Relative y-velocity profiles along the camber line for different rotor angular velocities at $t^* = 1.00$ at a) $x/C_x = 5\%$, b) $x/C_x = 48\%$, and c) $x/C_x = 95\%$.

does, however, vary with time, because the effect of the crossflow dissipates slightly during each vane-passing period.

In addition, small recirculation zones at the suction side and at the blade tip, similar to those found in the baseline case, were observed at smaller tip clearance heights and at lower turbulence intensities. These are due to the relative size of the separation bubble with tip clearance height. For these cases, the separation bubble occupies nearly half of the tip clearance region. As a result, the leakage flow will have a higher downward radial velocity as it negotiates around the separation bubble and the opposing flow near the shroud. At the suction side, small recirculation zones develop at the blade tip's suction side as the downward moving flow interacts and meets the flow passing over the suction side of the blade. It was observed that its size remains the same at all times.

Gas turbine designers are very interested in the heat transfer characteristics of the shroud. Results from CFD simulations are desirable because experimental methods are quite complex for data acquisition in the tip clearance region. In the present study, no heat transfer was considered in the simulations because it was not possible to obtain heat transfer calculations on the shroud using Nistar. In the meantime, the data provided in the present study could be extended to a heat transfer study of the shroud through the use of known heat transfer correlations. The aerodynamic data provided here could be inputted into heat transfer correlations to obtain heat transfer coefficients inside the tip clearance region.

Cooling flows should also be included in future simulations. Shrouds are usually cooled by the impingement of the flow, whereas blades are cooled externally through film cooling. In the present study, cooling flows were not included because [4] did not mention their presence. These cooling flows will affect the wall temperatures of both the blade and shroud, and so they will have a significant effect on the heat transfer in the tip leakage region. Nistar is able to implement cooling flows leaving the airfoil surface, but not those impinging on the shroud. Commercial software and preprocessors have the advantage of being able to model complex geometries that include impingement or film-cooling holes. Thus, commercial CFD software packages could be used for modeling tip leakage flows combined with additional cooling flows.

References

[1] Davis, R. L., Shang, T., Buteau, J., and Ni, R. H., "Prediction of 3-D Unsteady Flow in Multi-Stage Turbomachinery Using an Implicit Dual Time-Step Approach," AIAA Paper 96-2565, 1996.

[2] *FLUENT 6.2 User's Guide*, Fluent Inc., Lebanon, NH, 2005, Chaps. 9–12.

[3] Ni, R. H., "A Multiple-Grid Scheme for Solving the Euler Equations," *AIAA Journal*, Vol. 20, No. 11, 1982, pp. 1565–1571.

[4] Ni, R. H., and Bogoian, J. C., "Prediction of 3D-Multistage Turbine Flow Field Using a Multiple-Grid Euler Solver," AIAA Paper 89-0203, 1989.

[5] Radomsky, R. W., and Thole, K. A., "High Free-Stream Turbulence Effects on Endwall Heat Transfer for a Gas Turbine Stator Vane," *Journal of Turbomachinery*, Vol. 122, No. 4, 2000, pp. 699–708. doi:10.1115/1.1312807

[6] Chana, K. S., and Jones, T. V., "An Investigation on Turbine Tip and Shroud Heat Transfer," *Journal of Turbomachinery*, Vol. 125, 2003, pp. 513–520. doi:10.1115/1.1575253